communications earth & environment

ARTICLE

https://doi.org/10.1038/s43247-022-00450-5 OPEN

Climate warming amplified the 2020 record-breaking heatwave in the Antarctic Peninsula

Sergi González-Herrero [1,2]✉, David Barriopedro [3], Ricardo M. Trigo [4,5], Joan Albert López-Bustins[6] & Marc Oliva[6]

February 2020 was anomalously warm in the Antarctic Peninsula region and registered one of the most intense heatwaves ever recorded in Western Antarctica. The event featured unprecedented regional mean temperature anomalies (+4.5 °C) over the Antarctic Peninsula between 6 and 11 February 2020 and the highest local temperature of the continental Antarctic region. Taking flow analogs of the event from past (1950–1984) and recent (1985–2019) periods of the ERA5 reanalysis, here we quantify the role of recent climate change in the magnitude of this 6-day regional heatwave. Results show that 2020-like heatwaves over the Antarctic Peninsula are now at least ~0.4 °C warmer than in the past period, which represents a ~25% increase in magnitude. Given the observed atmospheric circulation conditions, the probability of experiencing 6-day regional mean anomalies above ~2 °C has increased ten times since 1950–1984. The aggravated severity of the event can be largely ascribed to long-term summer warming of the Antarctic Peninsula rather than recent atmospheric circulation trends.

[1] Antarctic Group, Agencia Estatal de Meteorología (AEMET), Barcelona, Spain. [2] Department of Applied Physics - Meteorology, Universitat de Barcelona, Barcelona, Spain. [3] Instituto de Geociencias (IGEO), Consejo Superior de Investigaciones Científicas – Universidad Complutense de Madrid, Madrid, Spain. [4] Instituto Dom Luiz (IDL), Faculdade de Ciências, Universidade de Lisboa, Lisboa, Portugal. [5] Departamento de Meteorologia, Universidade Federal do Rio de Janeiro, 21941-916 Rio de Janeiro, Brazil. [6] Department of Geography, Universitat de Barcelona, Barcelona, Spain. ✉email: sgonzalezh@aemet.es

In early February 2020, the Antarctic Peninsula (AP) and surrounding islands experienced one of the major heatwaves since reliable observations became available. During this period, a new all-time temperature record over the continental Antarctic region was observed on 6 February at Esperanza station (63°24'S, 57°00'W; 18.3 °C), and confirmed by a World Meteorological Organization (WMO) panel of atmospheric scientists[1]. The heatwave was widespread across the region from 6 to 11 February (Fig. 1) and other stations of the AP region also broke their temperature records[2]. The extremely high temperature anomalies were not restricted to the AP region alone, and Casey Station (Eastern Antarctica, Fig. 1) also exceeded its record high temperature in late January[3]. Synchronously, extensive surface ice melting occurred in the AP Ice Shelf during the 2019–2020 melt season[4,5]. The broad spatial extent and magnitude of extreme conditions underline the exceptionality of this event.

Similar to recent events that have affected other regions of the world (e.g., refs. [6,7]), extreme temperatures were associated with large-scale anomalous circulation patterns. The event was triggered by a high-pressure system on the Drake Passage that pushed warm and moist air from the Pacific Ocean to the AP region[8,9]. The warming induced by the anomalous atmospheric circulation was further amplified at local scales (Esperanza station) by the foehn effect prompted by leeward winds and the release of sensible heat[9,10]. Due to the high temperature values registered, the media gave extensive coverage to this event, often attributing it straightforwardly to climate change. However, to the best of our knowledge, no specific analysis, neither statistical nor dynamical, has been performed to date to confirm such attribution.

High temperature events in Antarctica must be framed within the recent climatic evolution of the continent. The AP region has experienced one of the fastest warmings on the planet since the 1950s[11–16]. However, part of this warming is linked to large-scale atmospheric circulation constraints, particularly the strengthening of the Southern Annular Mode (SAM)[13,17–20]. The climate of the region is also influenced by tropical and mid-latitude teleconnections[21–23], that together with the variations in the SAM produce large intra-decadal variability in AP temperatures[24,25], including relatively cooling periods within the long-term warming trend[14,26–29].

Although the influence of anthropogenic climate change on the generalized Antarctic warming is well established[13,16,30–33], its role in the occurrence of specific events in this continent has been barely explored. The 2019–2020 austral summer has been evaluated at seasonal and monthly scales[3,5,8] but not at the spatio-temporal scales of the heatwave event. Recently, Xu et al.[9] provided a comprehensive evaluation of the contributing physical mechanisms to the new local temperature record of Esperanza station, but without discussing its potential relationship to climate change. Here, we present the first assessment of the potential role played by recent climate change in the 2020 heatwave event considering the entire AP region. To that purpose, we use the analog method adopted in recent publications for other regions (e.g., refs. [34–36]). Based on reanalysis and observed datasets we provide evidence that the AP warming of the last decades has contributed to exacerbate the magnitude of the 2020 event.

Results

The 2020 summer (herein defined as the period from December 2019 to February 2020) was a warm season in Antarctica, with slightly warmer than average conditions over most of East Antarctica but extraordinary warm anomalies over the AP, West

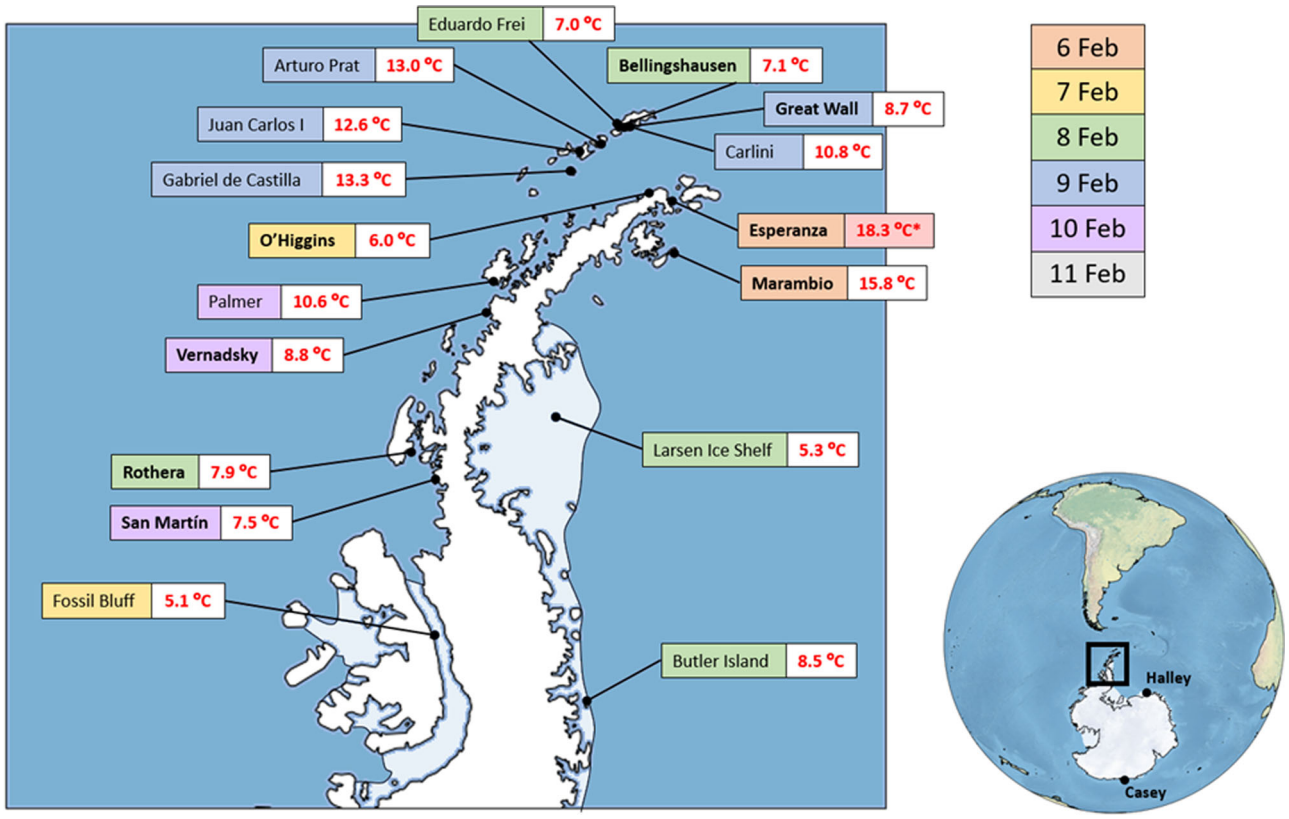

Fig. 1 Highest temperatures recorded during the 6–11 February 2020 heatwave. Highest temperature and date for the available stations of the Antarctic Peninsula and the 6–11 February 2020 period according the SYNOP messages. Squares include the station name and are filled with shading colors indicating the date when the highest temperature was observed. Names in bold identify the long-term stations employed for additional analyses. For the Esperanza station we show the record value reported by the WMO expert panel[1], which is slightly different to that inferred from SYNOP messages (18.4 °C).

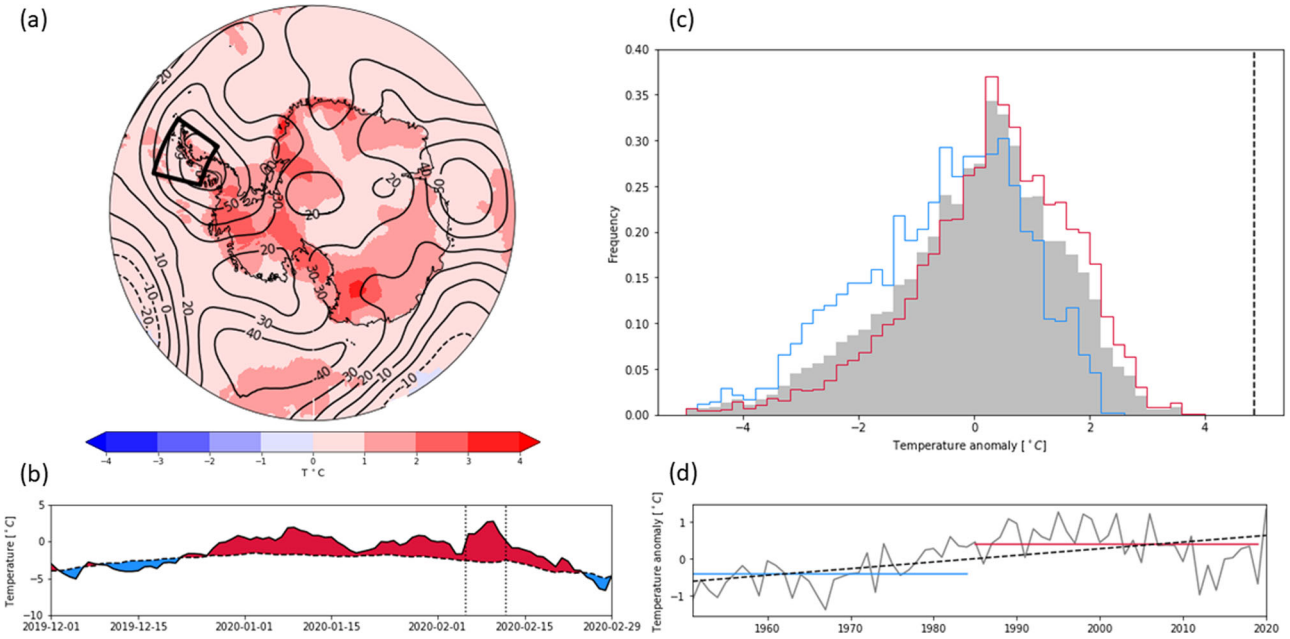

Fig. 2 Summer 2020 anomalies and climatological distribution and trends. a Z500 (contours; gpm) and T2m (shading; °C) anomalies for the 2020 summer (Dec–Feb) with the AP region highlighted. **b** Daily time series of regional mean AP T2m over land (in °C) for the 2020 summer (black solid line), with positive (negative) anomalies in red (blue). Dashed line shows the corresponding climatological values (1950–2019) and dotted vertical lines indicate the 6–11 Feb 2020 period. **c** Climatological (1950–2019) frequency distribution of the 6-day running mean series of AP T2m anomalies for all summer days of the 1950–2019 period (in °C, wrt 1950–2019). Blue and red lines show the corresponding distributions for the past (1950–1984) and recent (1985–2019) sub-periods, respectively. Vertical dashed line shows the 6-day mean AP T2m anomaly for 6–11 February 2020. **d** Time series of summer T2m anomalies for the AP region (°C, wrt 1950–2019). The dashed line indicates the linear trend. Blue and red lines show the climatological means for the past and recent sub-periods. Data source: ERA5 reanalysis.

Antarctica and Victoria Land (Fig. 2a), where 2-m temperature (T2m) anomalies exceeded 3 °C (see also the Data section). However, the warmest temperatures did not occur synchronously in all those regions (Figs. 1 and S1). In particular, the AP region experienced the warmest temperatures from 6 to 11 February 2020 (Fig. 2b). The highest local T2m (18.3 °C) was recorded at Esperanza station on 6 February[1,9]. However, this record did not correspond to the warmest day at the regional scale (10 February; Fig. 2b). Indeed, during the 6-day heatwave period there were four days with regionally averaged temperatures higher than those on 6 February according to the ERA5 reanalysis.

The early February 2020 AP heatwave was associated with a quasi-stationary high-pressure system over the Drake Passage. The event displayed exceptional time-averaged characteristics for the 6-day interval of 6–11 February, with local 500 hPa geopotential (Z500) and T2m anomalies above 300 gpm and 8 °C (Fig. 3a). Within the AP region, T2m anomalies were comparatively higher leeward of the AP mountain range, in agreement with the anomalous upwind westerlies set by the high-pressure system and the downslope Foehn winds (Fig. S2). During this period, the 6-day running mean T2m and Z500 settled new record values for the summer 1950–2020 distribution over most of the area (Fig. 3b, c), and the 6-day mean spatial average of T2m for the AP region was the highest ever recorded (Fig. 2c). The regional event occurred within a historical context of summer warming over the AP (Fig. 2d; 0.2 °C dec^{-1}, $p < 0.001$), which is also evident at shorter time-scales (compare the summer distributions of 6-day mean AP T2m for the first and second halves of the analyzed period in Fig. 2c).

Figure 4a (left panel) shows the mean AP T2m anomaly for 6–11 February (4.5 °C; black dot) and the corresponding distributions reconstructed from past (1950–1984; blue boxplot) and recent (1985–2019; red boxplot) flow analogs (see Methods). The spread of the distributions accounts for internal variability therefore indicating the possible outcomes that are compatible with the observed atmospheric circulation, as constrained by historical Z500 and mean sea level pressure (MSLP) fields. By construction, none of the analogs capture the outstanding amplitude of the 2020 AP heatwave, since the event was record-breaking. However, flow analogs of the 2020 AP heatwave are largely biased towards warm T2m anomalies during both sub-periods, indicating large influences of the atmospheric circulation, similar to those reported in other attribution studies of heatwave events[34–36]. The comparison of the past and recent distributions indicates that a similar flow configuration would have caused larger AP warming ($p < 0.001$) in recent (1.9 °C on average) than in past decades (1.5 °C). A greater difference is obtained for the warmest analogs (i.e., high percentiles of the distributions), which show AP T2m anomalies of up to 3.3 °C in the recent period and 2.6 °C for the past, yielding a 0.7 °C warming of the event in just the last three decades. The number of warm analogs, defined as those with AP T2m anomalies above 2 °C (the 95th percentile of the climatological distribution), is also much higher in the recent than in the past distribution (Fig. 4b).

To deep further into the magnitude of the event, we also assessed the contributions of different physical processes to the regional mean AP warming, namely horizontal temperature advection, adiabatic warming by subsidence and diabatic heating (see Methods). The AP temperature experienced small variations before the heatwave (Fig. 5a), and scaled abruptly at the beginning of the event (5 February), mainly due to warm horizontal advection, with a secondary contribution of diabatic heating (see green squares in Fig. 5b). The adiabatic term played a minor role in this escalation, likely reflecting the lack of organized subsidence during the development of the high-pressure system. For the remaining days of the event (6–9 February), AP temperatures kept at high values, with comparatively smaller

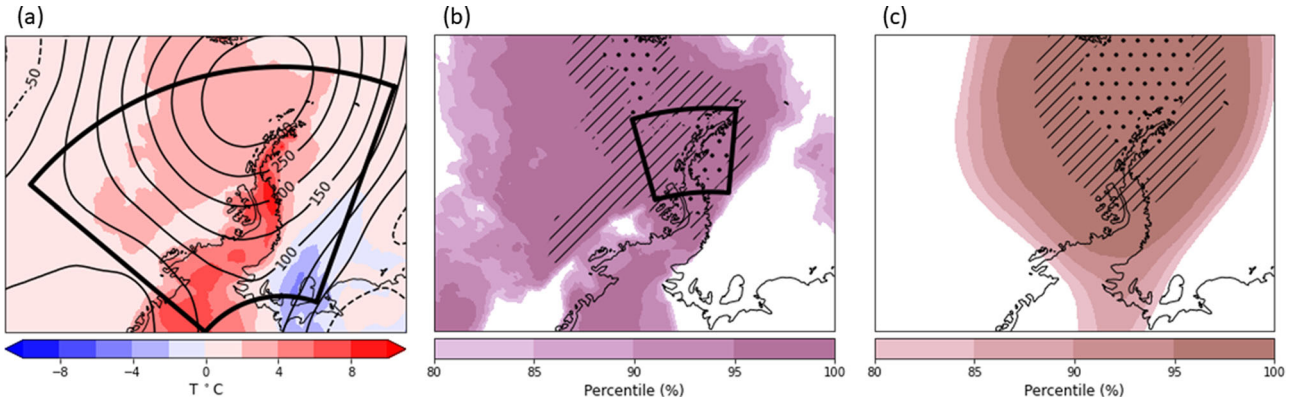

Fig. 3 Anomalies and percentiles of the 6–11 February 2020 heatwave. a Z500 (contours; in gpm) and T2m (shading; in °C) anomalies (wrt. 1950–2019) for 6–11 February 2020. **b**, **c** Percentiles of the 6–11 February 2020 mean (**b**) T2m and (**c**) Z500, with respect to the climatological distribution of 6-day running means obtained from all summer days of 1950–2019. Dashed and dotted regions indicate the 99th percentile and record-breaking values, respectively. The AN and AP regions are highlighted in (a) and (b), respectively. Data source: ERA5 reanalysis.

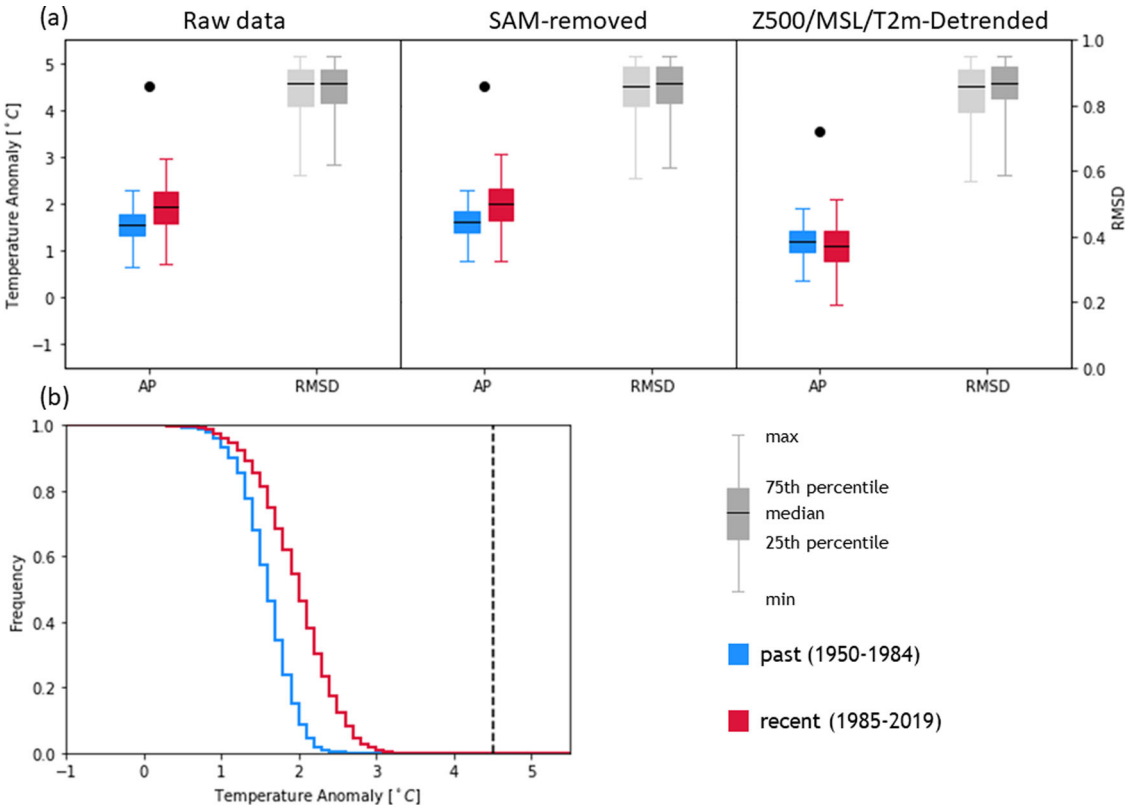

Fig. 4 Analog analysis of the 6–11 February 2020 heatwave. a Flow-conditioned distributions of 6-day mean AP T2m anomaly (colored whiskers; °C wrt. 1950–2019 in left y-axis) and normalized AN Z500/MSLP RMSD (grey whiskers; gpm in right y-axis) as reconstructed from analogs of the 2020 AP heatwave (6–11 February 2020). Blue and light grey whiskers show the distributions from past (1950–1984) analogs, while red and dark grey whiskers correspond to the recent sub-period (1985–2019). Left, central and right insets in (**a**) show the distributions obtained from the raw data, SAM-removed data, and detrended data respectively. Boxes denote the 25th–75th percentile ranges and whiskers span the 1st–99th percentiles. Black dot indicates the 6–11 February 2020 mean T2m anomaly in the AP region. **b** Cumulative distribution function with the relative frequency of past (blue) and recent (red) analogs displaying 6-day mean anomalies of AP T2m above a given threshold (x-axis). Data source: ERA5 reanalysis.

warming tendencies. Different to the growing phase, persistence was dominated by subsidence (Fig. 5a) associated with the quasi-stationary intense high-pressure system (Fig. S3), although sustained warm advection contributed to maintain the regional mean anomaly. When the whole event is considered (black dots in Fig. 5b), horizontal advection and adiabatic warming showed similar contributions to the AP warming. The evolution reconstructed with flow analogs (colored distributions in Fig. 5b) reproduces the observed balance of the contributing terms and hence the relevant mechanisms of the 2020 AP heatwave. The intensification of the 2020 AP heatwave is also consistent with increases in horizontal advection ($p < 0.001$) and adiabatic warming ($p < 0.001$) during recent analogs. For the same atmospheric configuration, a warmer atmosphere is expected to cause warmer advection as well as enhanced compression by thermal expansion and associated deepening of high pressure systems.

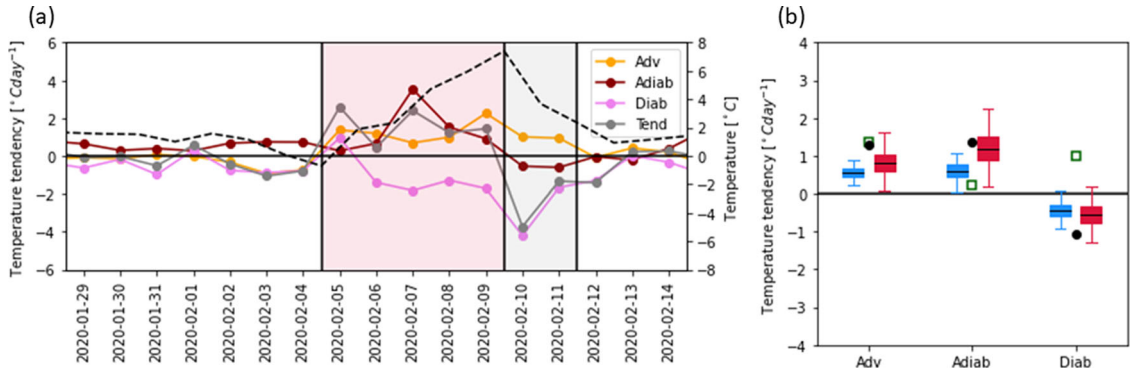

Fig. 5 Physical processes contributing to the 6–11 February 2020 heatwave. a Evolution of the observed AP temperature tendency at 975 hPa (*Tend*; in °C day^{-1}). The dashed gray line represents the mean AP absolute temperature at 975 hPa. Pink and grey areas indicate the warming (*Tend* > 0) and cooling (*Tend* < 0) phases of the 2020 AP heatwave, respectively. **b** Distributions of the mean AP temperature tendency (in °C day^{-1}) for each contributing term over the warming period (5–9 February 2020) of the 2020 AP heatwave, as reconstructed from past (1950–1984, blue whiskers) and recent (1985–2019, red whiskers) flow analogs. The contributing terms include horizontal temperature advection (*Adv*), adiabatic warming (*Adiab*) and diabatic heating (*Diab*). Black dots indicate the observed mean values for 5–9 February 2020, with green squares corresponding to the escalation phase (5 February 2020). Boxers and whiskers follow the same layout as in Fig. 4. Data source: ERA5 reanalysis.

On sub-regional scales, local processes associated with the leeward Foehn winds also contributed to the observed AP warming during the 2020 heatwave by increasing temperatures over the eastern half of the AP. This is supported by a partition analysis of analog days, which confirms an additional ~0.2 °C ($p < 0.001$) regional mean warming when flow analogs are accompanied by Foehn effect (FE; see Methods). Accordingly, FE-constrained analogs are also associated with significantly larger warm advection and adiabatic warming over the AP than non-Foehn (nFE) analog days. Ultimately, the enhancement of these drivers of AP warming during FE days can be traced back to subtle changes in the large-scale high-pressure system that prompt the favorable upwind conditions for the Foehn effect (Fig. S4). They include the strengthening of northwesterly winds over the AP and attendant transport of warm moist air masses, which have been related to Foehn warming downwind[4,37–39].

As the atmospheric circulation was key for the heatwave event (e.g., ref. [9]) and it is constrained by the flow analogs, the difference between the past and recent distribution of AP T2m anomalies (Fig. 4a) could in principle be attributed to thermodynamic changes. However, the Antarctic region has also experienced substantial dynamical changes –here defined as those in atmospheric circulation– that may affect the characteristics of the analogs, therefore potentially contributing to the differences in the reconstructed distributions of AP T2m anomalies. Although the distribution of root-mean squared differences (RMSD) of Z500/MSLP is similar for the past and recent analogs (Fig. 4a; grey boxplots), the frequency of analogs has decreased significantly through the 1950–2019 period ($p < 0.01$; Fig. S5a). This trend may reflect recent dynamical changes, the most notable ones in the AP region being those associated with the summer SAM trend, and attendant decreases in the frequency of summer ridge patterns[40,41]. However, we did not find a significant correlation between SAM and the summer frequency series of analogs ($r = -0.168$; $p > 0.05$), as one would expect from a SAM driving. Furthermore, the correlation coefficient is similar after detrending these series ($r = -0.165$; $p > 0.05$), indicating that if there is any interannual effect of the SAM on the analog frequency it has changed little with its increasing trend. Finally, the trend in the frequency of analogs remains unaltered after removing the effect of SAM-congruent trends on the mean circulation fields (Fig. S5a). If any, the SAM trend has counteracted the deepening trend of high-pressure systems: the magnitude of Z500 anomalies during recent analogs is lower than would have been without a SAM trend (Fig. S5b). In spite of this, the analog-based distributions of AP T2m anomalies change little after accounting for the trend in the summer SAM: in absence of changes in the SAM, the 2020 AP heatwave would still have been ~0.6 °C warmer now than in the past (Fig. 4a, middle panel). Therefore, we hypothesize that there have been limited influences of long-term SAM changes in the recent intensification of 2020-like AP heatwaves.

To explore whether long-term dynamical changes other than the SAM trend can explain the warming signal, we repeated the analysis by removing the regional mean summer trend in Z500 and MSLP (and not only that due to SAM changes). The results are similar to those obtained with the SAM-detrending experiment (not shown), confirming that long-term dynamical trends in the AP region have been largely driven by the SAM. In particular, the reconstructed T2m distributions for the 2020 AP heatwave still preserve much of their original differences (Fig. S6a). Therefore, dynamical trends, either associated or not with the increasing SAM cannot explain the reported warming of 2020-like AP heatwaves. On the contrary, when the regional mean AP T2m trend is removed from the data (either in isolation or along with the AN Z500/SLP trend), the differences between the past and recent analog distributions disappear (Fig. 4a, right panel). These results point to major influences of long-term regional mean warming in exacerbating the magnitude of the 2020 AP heatwave. This summer AP warming cannot be explained by atmospheric circulation changes (the SAM trend) either, which stresses the importance of thermodynamical aspects of climate change.

Discussion and conclusions

Previous studies have described the extreme conditions that affected the Antarctica during the 2019–2020 summer, focusing on either monthly mean temperatures[3,8,37] or daily extreme temperatures at specific locations (namely the Esperanza station; ref. [9]). Although complementary, our analysis differs from these previous assessments by adopting an event approach that focuses on the February 2020 heatwave event (6–11 February 2020) and the entire AP, including the new all-time daily surface temperature record in the continental Antarctic region.

An event of this magnitude has been unprecedented over the region in the last 70 years. It was associated with the occurrence of a large quasi-stationary high-pressure pattern at the northern extreme of the AP region. The warm advection accounted for a substantial fraction of the abrupt regional mean temperature

escalation, which was additionally assisted by adiabatic warming during the maintenance phase. The anomalous circulation also contributed to the event magnitude by setting the favorable upwind conditions for Foehn winds and associated leeward warming over the eastern half of the AP. Despite setting new all-time records beyond the available instrumental period, we find that atmospheric circulation events similar to the 2020 AP heatwave would have been colder under past climate conditions. Specifically, recent changes have exacerbated the severity of this class of event by at least 0.4 °C ($p < 0.001$), which represents ~25% of its historical magnitude, and the probability of experiencing a 6-day event with AP T2m anomaly above 2 °C is now ten times larger than just a few decades ago.

Our results suggest that changes associated with the increasing trend in the summer SAM played a minor role in the exceptional magnitude of the 2020 AP heatwave. Additional analyses yield a similar small influence of overall long-term trends in the large-scale circulation. In agreement with previous studies reporting a decrease in the frequency of summer ridges[4041], we find a declining frequency of high-pressure patterns similar to that took place at the time of the 2020 AP heatwave, along with an increasing amplitude of such atmospheric circulation patterns. However, we do not find convincing evidences for a SAM driving of these changes. If any, the SAM trend acted against the climate change signal by weakening the deepening rate of these high-impact systems. Accordingly, when SAM-induced trends are disregarded, we obtain a slightly stronger climate change signal in the event magnitude (0.6 °C). Therefore, recent changes in the atmospheric circulation cannot explain the exacerbated magnitude of this extreme event, and hence the climate change signal detected herein should be largely ascribed to thermodynamic changes. This is supported by additional experiments where the regional mean warming signal is removed from the data.

Although our results are robust to methodological choices, we acknowledge potential limitations and assumptions in the adopted approach, some of which are inherent to the analog method (e.g., refs. [34,42]). They include the relatively short periods to search for good enough flow analogs, and the inability to disentangle specific anthropogenic factors from the overall climate change signal[42,43]. Regarding the latter, many environmental changes have occurred in the AP region since the mid-20th century[16,44]. The circumpolar circulation has contracted with the predominance of the positive phase of the SAM resulting from both the greenhouse gases increase and stratospheric ozone depletion[32,45,46]. Internal variability counteracted the warming of the AP region in the early 21st century[26,27] but this hiatus has been hypothesized to end[29]. A recent study has demonstrated that when the SAM-congruent trend is removed from the observed surface temperature trend, a background warming trend (consistent with the overall global warming) is observed over the past 60 years[13], therefore linking regional mean AP warming with anthropogenic factors[33]. In agreement with the climate change signal detected herein for the 2020 AP heatwave event, long-term trends in warm extremes at Rothera and Halley stations have also been associated with accelerated regional warming[47]. The short record of observations, the large interannual to decadal variability of the AP region[14,48] and the multiplicity of drivers (e.g., SAM, the Amundsen Sea Low, El Niño Southern Oscillation (ENSO), sea ice variations; refs. [24,48–51]) make it difficult to attribute this summer AP warming to specific processes (e.g., water vapor and albedo feedbacks, enhanced warm air mass intrusions from extratropics, etc.), which still remain poorly explored and should be subject of future studies. In spite of this, the link between the AP warming and the global warming reported in previous studies (e.g., refs. [13,16,33,52]), and the projected increases in the frequency and/or severity of Antarctic heatwaves under higher concentrations of greenhouse gases[53] lets us anticipate that the warming signal detected at the event scale can be largely attributed to anthropogenic factors. We encourage additional supporting analyses based on different datasets, attribution methods and climate models of diverse complexity.

Data and methods

Observational data. Station-based temperatures in the AP were obtained from the SYNOP messages (Fig. 1). Observational daily mean temperature anomalies (see Fig. S1) were computed with respect to the climatological (1950–2019) mean temperature of the summer season (December-January-February) using high-quality long-term series with more than 30 years of observations (Fig. 1 in bold) from the SCAR MET-READER surface station dataset[54]. This dataset was also used to validate temperature reanalysis data. Monthly mean values of 500 hPa geopotential height (Z500) at 00 and 12 UTC for four stations available in the AP region (Bellingshausen, Marambio, Faraday/Vernadsky and Rothera) were also retrieved from the SCAR MET-READER upper air dataset to validate the reanalysis data.

Reanalysis data. The state-of-the-art ECMWF ERA5 reanalysis[55] was used in this study for the 1950–2020 period, which allows the assessment of changes during the last decades. This reanalysis has been extensively validated in Antarctica, presenting the best performance with respect to other reanalysis products[56–58]. To reduce the uncertainty, especially for the pre-satellite era, we used the 10-ensemble member mean fields provided by ERA5. We retrieved several meteorological 3-hourly variables with a horizontal resolution of 0.5°, including 2-meter temperature (T2m), mean sea level pressure (MSLP) and 500 hPa geopotential height (Z500). The 3-hourly values of each day (00, 03, 06, 09, 12, 15, 18 and 21 UTC) were averaged to produce daily means. Z500 and T2m fields were validated using radiosonde and station data for the 1950–1984 and 1985–2019 sub-periods. For the validation process of the reanalysis product we used the available observations all year-round (Fig. S7), as well as the summer months only (Table S1). These datasets compare well, with slightly lower mean absolute error and higher correlation coefficients for the more recent sub-period. However, the performance of ERA5 drops noticeably in the first years, prior to the deployment of most Antarctic stations during the 3rd International Polar Year (1950–1956). We confirmed that excluding those years does not introduce significant changes in the results. The sign of Z500 and T2m biases varies across the stations, indicating that there is not a systematic deviation over the AP region (Table S1).

Analog method. To evaluate the role played by climate change in this event we used the analog method for the period comprised between 6 and 11 February 2020, which exhibited the largest T2m anomalies (above 3.5 °C) over the AP region [62–70°S 76–55°W] (Fig. 2c) and many of the observational stations (Fig. S1). Anomalies are computed with respect to the climatological (1950–2019) mean of the summer season. This attribution method infers the probability distribution of a target field from the atmospheric circulation during the event (e.g., ref. [43], and references therein) and has been extensively used to evaluate changes in the magnitude of major European heatwaves (*e.g.*[35,36,59,60]). The method assumes a key role of the atmospheric circulation in the extreme event, which was already demonstrated by ref. [9] for the 2020 heatwave at Esperanza station. The atmospheric circulation and the heatwave event were characterized by the daily mean MSLP and Z500 fields over the [55°–78°S; 120–40°W] region (AN region hereafter) and by regional means of daily mean T2m over the AP region, respectively. These daily fields

were derived from 3-hourly values of the 10-ensemble mean of ERA5. The regional mean T2m series for the AP region was computed from land grid points only (including ice shelves) by using a land-sea mask. The AN region was defined to span the main weather systems that affect the AP, such as the summer Amundsen-Bellingshausen Sea Low. These atmospheric circulation fields over AN capture well the anomalous high-pressure system associated with the event. We obtain similar results if the MSLP or Z500 fields are used in isolation to constrain the atmospheric circulation, and if other target fields (e.g., 850 hPa temperature) are employed to characterize the amplitude of the event.

We searched for historical flow analogs of the heatwave event in every summer of the 1950–2019 period by computing the RMSD of the normalized MSLP and Z500 anomaly fields over the AN area (after weighting by the square root of the cosine of the latitude). Then, for each day of the heatwave period, we identified flow analog days as those with RMSD < 0.9 standard deviation, which roughly corresponds to the 5th percentile of the distribution. The regional mean T2m anomaly distribution of the AP region was reconstructed from analog days of the past (1950–1984) and recent (1985–2019) sub-periods separately. These distributions were obtained by picking randomly the anomalous T2m of one of their analog days, and repeating this process $N = 5{,}000$ times. This yields a circulation-constrained temperature distribution for the past and recent sub-periods, i.e., the AP T2m anomalies that could be expected in these sub-periods under atmospheric circulation conditions similar to those recorded at the time of the event. We tested the sensitivity of the results to methodological choices, including the pool size of analogs (i.e., different RMSD thresholds), the definition of flow analogs (e.g., by setting a fixed number of best analogs), the selection of the spatial and temporal domains of the event (AP and AN regions), and the timing of analogs (the summer months of the pool), obtaining similar results.

To account for long-term changes in the dynamical and thermodynamic fields, the analog method was also applied after removing the linear trend of the summer mean AN MSLP/Z500 and AP T2m separately. The detrended value for each summer was applied to all days of that summer (and, in the case of MSLP and Z500, to all grid points of the AN region) to obtain the detrended daily series of atmospheric circulation fields and AP T2m.

As an additional experiment, we also removed the mean changes in AN MSLP/Z500 and AP T2m associated with the increasing trend in the summer SAM. The SAM index was computed from monthly ERA5 data, following Gong and Wang[61]:

$$SAM = MSLP^*_{40^\circ S} - MSLP^*_{65^\circ S} \quad (1)$$

where $MSLP^*$ is the normalized zonal mean MSLP at the given latitude. The summer SAM series was obtained by averaging the monthly values of each summer. To determine the SAM-induced trend in the time series of AN MSLP/Z500 and AP T2m, we used the method developed by Thompson et al.[62], which has already been applied to quantify the SAM influence in Antarctic temperature trends[13]. We first linearly regressed the detrended summer series onto the detrended SAM index over the 1950–2019 period, and multiplied the regression coefficient by the SAM trend. The resulting slope accounts for the trend in the regional mean series that is congruent with that in the SAM. As in the detrended exercises described above, this trend was removed from the original daily series of MSLP/Z500 and AP T2m, obtaining the residuals, which retain the component of the regional mean summer trend that is linearly independent of the SAM index. The detrended and SAM-removed experiments yielded similar results if the process is applied to each grid point, therefore accounting for spatial changes in the patterns, rather than to the spatially averaged series of AN MSLP/Z500 and AP T2m.

Thermodynamic equation and associated physical processes. To assess the contribution of different physical processes to the escalation and maintenance of regional mean temperatures during the 2020 AP heatwave, we used the thermodynamic equation, which governs the temperature tendency:

$$\underbrace{\frac{\Delta T}{\Delta t}}_{Tend} = \underbrace{-\vec{v}\cdot\nabla_p T}_{Adv} \underbrace{-\omega\frac{T}{\theta}\frac{\partial\theta}{\partial p}}_{Adiab} + \underbrace{Q}_{Diab} \quad (2)$$

where $\vec{v}$ is the horizontal wind, T the temperature, ω the vertical velocity in pressure coordinates, θ the potential temperature and p the pressure. Equation 2 was evaluated at 975 hPa (we obtain similar results at 950 hPa; not shown), which is justified by its proximity to the surface and the need of computing vertical gradients. *Tend* represents the daily temperature tendency, i.e., the forward difference of 975 hPa temperature (T975) between the beginning and the end of the day at 00 UTC. *Adv* is the T975 advection by the horizontal wind at the same pressure level (the zonal and meridional wind fields, U975 and V975). *Adiab* represents the adiabatic heating due to vertical motion (w975) and thermal stratification (the vertical gradient is estimated from temperature at 950 hPa and 1000 hPa pressure levels, T950 and T1000). Finally, *Diab* shows the change in temperature due to diabatic processes. The three first components were computed at each grid point before averaging over the AP region. The *Diab* term, encompassing radiative and heating fluxes, does not allow an explicit computation at the required pressure level and was estimated as the residual of Eq. 2, although it might also include other factors such as sub-grid turbulent mixing or numerical errors. With all, the contribution of this term to the event was found to be of secondary importance (lower than *Adv*) and more frequently negative (i.e., counteracting additional warming). We used the relative contribution of each term to evaluate the dominant mechanisms during the AP warming period (5–9 February; i.e., when the *Tend* term was positive), which includes the building up and maintenance phases of the event. These terms were also evaluated for the flow analogs of the 2020 AP heatwave. As the *Tend* term also depends on the specific pattern preceding the analog one, which may be different to the observed one, the selection of analogs for this analysis was limited to those with $Tend > 0$ (as in observations), although the results do not change if all analogs are used instead.

Foehn effect. To diagnose the occurrence of Foehn winds downwind of the AP cordillera, we calculated the mountain Froude number in the AP region:

$$Fr = \frac{U_{in}}{NH} \quad (3)$$

where H is the mountain height, taken as 1000 m, which is the approximated maximum elevation of the AP region in ERA5, and U_{in} is the regional mean wind speed blowing perpendicular to the mountain, herein evaluated at 975 hPa. As the AP mountain range stretches roughly from SW to NE, we approximated U_{in} from the wind speed in the NW-SE direction, with positive values denoting northwesterly winds and negative values denoting southeasterly winds:

$$U_{in} = U975 \cdot \cos(45^\circ) - V975 \cdot \sin(45^\circ) \quad (4)$$

Finally, N is the Brunt-Väisälä frequency in pressure coordinates:

$$N^2 = -\frac{\rho g^2}{\theta}\frac{\partial\theta}{\partial p} \quad (5)$$

where ρ is the density of the air, g is the gravity acceleration, θ the potential temperature and p the pressure. Equation 5 was

evaluated at 975 hPa, using the regional mean T950 and T1000 fields over the AP region to calculate the derivative.

Summer days were classified into those with Foehn effect (FE) and non-Foehn effect (nFE). To do this, we followed King et al.[63], who showed that Foehn conditions in Larsen C are often associated with $Fr \geq 0.2$. Using this threshold, all but one day of the 2020 AP heatwave displayed Foehn conditions. Analog days of the 2020 AP heatwave were also classified into FE and nFE days to estimate the potential effects of Foehn winds in the magnitude of the event and the associated changes in its major drivers (*Adv* and *Adiab*). FE days make up 62% of the 2020 AP heatwave analog days, which is significantly higher than the climatological frequency of summer days with FE (~25%), confirming that FE is to a large extent conditioned by the large-scale atmospheric circulation. Accordingly, we obtain qualitatively similar results to those reported in the main text if only FE analog days are used to constrain the 2020 AP heatwave (e.g., Fig. S6b).

Data availability

Data used in this study are publicly accessible. SYNOP messages can be obtained from https://www.ogimet.com/. Observational data from SCAR MET-READER can be downloaded from: https://legacy.bas.ac.uk/met/READER/. ERA5 dataset can be downloaded from: https://cds.climate.copernicus.eu/.

Code availability

Main Python codes used in this study are available in the following Githut repository: https://github.com/sergigonzalezh/2020AntarcticHeatwave_attribution_analogs. Additional codes are available upon request.

Received: 25 October 2021; Accepted: 10 May 2022;
Published online: 27 May 2022

References

1. Rocha, F. M. et al. WMO evaluation of two extreme high temperatures occurring in february 2020 for the Antarctic Peninsula Region. *Bull. Am. Meteorol. Soc.* **1**, 1–20 (2021).
2. AEMET. *Informe climatológico de las Bases Antárticas Españolas 2020.* https://antartida.aemet.es/index.php?pag=informes&bol=12 (2021).
3. Robinson, S. A. et al. The 2019/2020 summer of Antarctic heatwaves. *Global Change Biol.* **26**, 3178–3180 (2020).
4. Banwell, A. F. et al. The 32-year record-high surface melt in 2019/2020 on the northern George VI Ice Shelf, Antarctic Peninsula. *Cryosphere* **15**, 909–925 (2021).
5. Bevan, S., Luckman, A., Hendon, H. & Wang, G. The 2020 Larsen C Ice Shelf surface melt is a 40-year record high. *Cryosphere* **14**, 3551–3564 (2020).
6. Barriopedro, D., Fischer, E. M., Luterbacher, J., Trigo, R. M. & García-Herrera, R. The hot summer of 2010: Redrawing the temperature record map of Europe. *Science* **332**, 220–224 (2011).
7. Sousa, P. M., Trigo, R. M., Barriopedro, D., Soares, P. M. M. & Santos, J. A. European temperature responses to blocking and ridge regional patterns. *Clim. Dyn.* **50**, 457–477 (2018).
8. Clem, K., Bozkurt, D., Kennet, D., King, J. & Turner, J. Central tropical Pacific convection drives extreme high temperatures and surface melt on the Larsen ice shelf. https://doi.org/10.21203/rs.3.rs-712751/v1 (2021).
9. Xu, M. et al. Dominant role of vertical air flows in the unprecedented warming on the Antarctic Peninsula in February 2020. *Commun. Earth Environ* **2**, 1–9 (2021).
10. Turner, J. et al. Extreme temperatures in the Antarctic. *J. Clim.* **34**, 2653–2668 (2021).
11. Steig, E. J. et al. Warming of the Antarctic ice-sheet surface since the 1957 International Geophysical Year. *Nature* **457**, 459–462 (2009).
12. Carrasco, J. F. Decadal changes in the near-surface air temperature in the western side of the Antarctic Peninsula. *Atmos. Clim. Sci.* **03**, 275–281 (2013).
13. Jones, M. E. et al. Sixty years of widespread warming in the southern middle and high latitudes (1957–2016). *J. Clim.* **32**, 6875 (2019).
14. Gonzalez, S. & Fortuny, D. How robust are the temperature trends on the Antarctic Peninsula? *Antarct. Sci.* **30**, 322–328 (2018).
15. Vaughan, D. G. et al. Recent rapid regional climate warming on the Antarctic Peninsula. *Clim. Change* **60**, 243–274 (2003).
16. Jones, J. M. et al. Assessing recent trends in high-latitude Southern Hemisphere surface climate. *Nat. Clim. Change* **6**, 917–926 (Nature Publishing Group, 2016).
17. Thompson, D. W. J. & Solomon, S. Interpretation of recent Southern Hemisphere climate change. *Science* **296**, 895–899 (2002).
18. van den Broeke, M. R. & van Lipzig, N. P. M. Factors controlling the near-surface wind field in Antarctica. *Mon. Weather Rev.* **131**, 733–743 (2003).
19. Turner, J. et al. Record low surface air temperature at Vostok station, Antarctica. *J. Geophys. Res. Atmos.* **114**, 24102 (2009).
20. Orr, A. et al. A 'low-level' explanation for the recent large warming trend over the western Antarctic Peninsula involving blocked winds and changes in zonal circulation. *Geophys. Res. Lett.* **31**, L06204 (2004).
21. Ding, Q. & Steig, E. J. Temperature change on the Antarctic Peninsula linked to the tropical Pacific. *J. Clim.* **26**, 7570–7585 (2013).
22. Fogt, R. L. & Bromwich, D. H. Decadal variability of the ENSO teleconnection to the high-latitude south pacific governed by coupling with the Southern Annular mode. *J. Clim.* **19**, 979–997 (2006).
23. Sato, K., Inoue, J., Simmonds, I. & Rudeva, I. Antarctic Peninsula warm winters influenced by Tasman Sea temperatures. *Nat. Commun.* **12**, 1497 (2021).
24. Clem, K. R., Renwick, J. A., McGregor, J. & Fogt, R. L. The relative influence of ENSO and SAM on Antarctic Peninsula climate. *J. Geophys. Res.* **121**, 9324–9341 (2016).
25. Fogt, R. L., Bromwich, D. H. & Hines, K. M. Understanding the SAM influence on the South Pacific ENSO teleconnection. *Clim. Dyn.* **36**, 1555–1576 (2011).
26. Oliva, M. et al. Recent regional climate cooling on the Antarctic Peninsula and associated impacts on the cryosphere. *Sci. Total Environ.* **580**, 210–223 (2017).
27. Turner, J. et al. Absence of 21st century warming on Antarctic Peninsula consistent with natural variability. *Nature* **535**, 411–415 (2016).
28. Parkinson, C. L. A 40-y record reveals gradual Antarctic sea ice increases followed by decreases at rates far exceeding the rates seen in the Arctic. *Proc. Natl. Acad. Sci. USA* **116**, 14414–14423 (2019).
29. Carrasco, J. F., Bozkurt, D. & Cordero, R. R. A review of the observed air temperature in the Antarctic Peninsula. Did the warming trend come back after the early 21st hiatus? *Polar Sci.* **28**, 100653 (2021).
30. Quetelard, H. et al. Extreme weather: World-record rainfalls during tropical cyclone gamede. *Bull. Am. Meteorol. Soc.* **90**, 603–608 (2009).
31. Carril, A. F., Menéndez, C. G. & Navarra, A. Climate response associated with the Southern Annular Mode in the surroundings of Antarctic Peninsula: A multimodel ensemble analysis. *Geophys. Res. Lett.* **32**, 1–5 (2005).
32. Fogt, R. L. & Marshall, G. J. The Southern Annular Mode: Variability, trends, and climate impacts across the Southern Hemisphere. *Wiley Interdisciplinary Reviews: Clim. Change* **11**, e652 (2020).
33. Gillett, N. P. et al. Attribution of polar warming to human influence. *Nat. Geosci.* **1**, 750–754 (2008).
34. Yiou, P. et al. A statistical framework for conditional extreme event attribution. *Adv. Stat. Climatol. Meteorol. Oceanogr* **3**, 17–31 (2017).
35. Barriopedro, D., Sousa, P. M., Trigo, R. M., García-Herrera, R. & Ramos, A. M. The exceptional Iberian heatwave of summer 2018. *Bulletin of the American Meteorological Society* **101**, S29–S34 (2020).
36. Sousa, P. M. et al. Distinct influences of large-scale circulation and regional feedbacks in two exceptional 2019 European heatwaves. *Commun. Earth Environ* **1**, 1–13 (2020).
37. Clem, K., MacFerrin, M., Kennet, D. & Bozkurt, D. Sidebar 6.1: Record warmth and surface 327 melt on the Antarctic Peninsula in February 2020. In State of the Climate 2020: Antarctica and the Southern Ocean (eds S. Stammerjohn & T. Scambos) *Bull. Am. Meteorol. Soc.* 328–329 (2021).
38. Bozkurt, D., Rondanelli, R., Marín, J. C. & Garreaud, R. Foehn Event Triggered by an Atmospheric River Underlies Record-Setting Temperature Along Continental Antarctica. *J. Geophys. Res. Atmos.* **123**, 3871–3892 (2018).
39. Wille, J. D. et al. Intense atmospheric rivers can weaken ice shelf stability at the Antarctic Peninsula. *Commun Earth Environ* **3**, 90 (2022).
40. Gonzalez, S., Vasallo, F., Recio-Blitz, C., Guijarro, J. A. & Riesco, J. Atmospheric patterns over the Antarctic Peninsula. *J. Clim.* **31**, 3597–3608 (2018).
41. Marín, J. C., Bozkurt, D. & Barrett, B. S. Atmospheric blocking trends and seasonality around the Antarctic Peninsula. *J. Clim.* **1**, 1–58 (2022).
42. Harrington, L. J., Otto, F. E. L., Cowan, T. & Hegerl, G. C. Circulation analogues and uncertainty in the time-evolution of extreme event probabilities: evidence from the 1947 Central European heatwave. *Clim. Dyn.* **53**, 2229–2247 (2019).
43. Stott, P. A. et al. Attribution of extreme weather and climate-related events. *Wiley Interdiscip. Rev. Clim. Chang.* **7**, 23–41 (2016).
44. Turner, J. et al. Antarctic climate change and the environment: An update. *Polar Rec. (Gr. Brit)* **50**, 237–259 (2014).

45. Marshall, G. J., Di Battista, S., Naik, S. S. & Thamban, M. Analysis of a regional change in the sign of the SAM-temperature relationship in Antarctica. *Clim. Dyn.* **36**, 277–287 (2011).
46. Ivanciu, I., Matthes, K., Wahl, S., Harlaß, J. & Biastoch, A. Effects of prescribed CMIP6 ozone on simulating the Southern Hemisphere atmospheric circulation response to ozone depletion. *Atmos. Chem. Phys.* **21**, 5777–5806 (2021).
47. Prete, G., Capparelli, V., Lepreti, F. & Carbone, V. Accelerated climate changes in weddell sea region of antarctica detected by extreme values theory. *Atmos. 2021* **12**, 209 (2021).
48. Turner, J. et al. Antarctic temperature variability and change from station data. *Int. J. Climatol.* **40**, 2986–3007 (2020).
49. Raphael, M. N. et al. The Amundsen sea low: Variability, change, and impact on Antarctic climate. *Bull. Am. Meteorol. Soc.* **97**, 111–121 (2016).
50. Marshall, G. J., Orr, A., van Lipzig, N. P. M. & King, J. C. The impact of a changing Southern Hemisphere Annular Mode on Antarctic Peninsula summer temperatures. *J. Clim* **19**, 5388–5404 (2006).
51. Schneider, D. P., Deser, C. & Okumura, Y. An assessment and interpretation of the observed warming of West Antarctica in the austral spring. *Clim. Dyn.* **38**, 323–347 (2012).
52. Thomas, E. R., Dennis, P. F., Bracegirdle, T. J. & Franzke, C. Ice core evidence for significant 100-year regional warming on the Antarctic Peninsula. *Geophys. Res. Lett.* **36**, 20704 (2009).
53. Feron, S. et al. Warming events projected to become more frequent and last longer across Antarctica. *Sci. Reports 2021 111.* **11**, 1–9 (2021).
54. Turner, J. et al. The SCAR READER project: Toward a high-quality database of mean Antarctic meteorological observations. *J. Clim.* **17**, 2890–2898 (2004).
55. Hersbach, H. et al. The ERA5 global reanalysis. *Q. J. R. Meteorol. Soc.* **146**, 1999–2049 (2020).
56. Gossart, A. et al. An evaluation of surface climatology in state-of-the-art reanalyses over the Antarctic Ice Sheet. *J. Clim.* **32**, 6899–6915 (2019).
57. Tetzner, D., Thomas, E. & Allen, C. A validation of ERA5 reanalysis data in the southern antarctic peninsula—Ellsworth land region, and its implications for ice core studies. *Geosciences* **9**, 289 (2019).
58. Zhu, J. et al. An assessment of ERA5 reanalysis for antarctic near-surface air temperature. *Atmosphere (Basel)* **12**, 217 (2021).
59. Jézéquel, A., Yiou, P. & Radanovics, S. Role of circulation in European heatwaves using flow analogues. *Clim. Dyn.* **50**, 1145–1159 (2018).
60. Sánchez-Benítez, A., García-Herrera, R., Barriopedro, D., Sousa, P. M. & Trigo, R. M. June 2017: The earliest European Summer Mega-heatwave of Reanalysis period. *Geophys. Res. Lett.* **45**, 1955–1962 (2018).
61. Gong, D. & Wang, S. Definition of Antarctic oscillation index. *Geophys. Res. Lett.* **26**, 459–462 (1999).
62. Thompson, D. W. J., Wallace, J. M. & Hegerl, G. C. Annular modes in the extratropical circulation. Part II: Trends. *J. Clim.* **13**, 1018–1036 (2000).
63. King, J. C. et al. The Impact of Föhn Winds on Surface Energy Balance During the 2010–2011 Melt Season Over Larsen C Ice Shelf, Antarctica. *J. Geophys. Res. Atmos.* **122**, 12062–12076 (2017).

Acknowledgements

We thank David Bromwich for his useful comments and discussions on this research. We want to acknowledge the contribution of the two anonymous reviewers, which provided constructive comments that helped to substantially improve the final form of this manuscript. The AEMET Antarctic program is supported by the Ministerio para la Transición Ecológica y Reto Demográfico and Ministerio de Ciencia e Innovación of the Spanish Goverment. Research activities of S.G. and M.O. are partly funded by ANTALP Research Group, Generalitat de Catalunya. S.G. is supported by the Ministerio de Ciencia e Innovación project – PID2020-116520RB-I00 (MICROAIRPOLAR2) and RTI2018-098693-B-C32 (WISE-PreP). M.O. is supported by the Ramón y Cajal Program (RYC-2015-17597) and the NUNANTAR (PTDC/CTA-GFI/32002/2017) from the Fundação para a Ciência e a Tecnologia of Portugal. D.B. acknowledges support from the H2020 EU project CLINT (Grant Agreement No. 101003876). R.M.T. was supported of the Portuguese Foundation for Science and Technology through the FCT – project JPIO-CEANS/0001/2019 (ROADMAP). This research is part of the CSIC Interdisciplinary Thematic Platform (PTI) Clima y Servicios Climáticos (PTI-CLIMA) and POLARCSIC (PTI-POLAR) activities.

Author contributions

S.G.H. conceived the idea for the study, performed the calculations and produced the figures. S.G.H., D.B., R.M.T., A.L.B., and M.O. contributed in interpreting and discussing the results and writing the manuscript.

Competing interests

The authors declare no competing interests.

Additional information

Supplementary information The online version contains supplementary material available at https://doi.org/10.1038/s43247-022-00450-5.

Correspondence and requests for materials should be addressed to Sergi González-Herrero.

Peer review information *Communications Earth & Environment* thanks the anonymous reviewers for their contribution to the peer review of this work. Primary Handling Editor: Heike Langenberg. Peer reviewer reports are available.

Reprints and permission information is available at http://www.nature.com/reprints

Publisher's note Springer Nature remains neutral with regard to jurisdictional claims in published maps and institutional affiliations.